IOP Publishing Flex. Print. Electron. 6 (2021) 025009 https://doi.org/10.1088/2058-8585/ac03be

Flexible and Printed Electronics

PAPER

Screen printed chipless RFID tags on packaging substrates

Parya Fathi[1], Sika Shrestha[1], Ramprakash Yerramilli[1], Nemai Karmakar[1] and Sankar Bhattacharya[2]

[1] Department of Electrical and Computer System Engineering, Monash University, Clayton, VIC, Australia
[2] Department of Chemical Engineering, Monash University, Clayton, VIC, Australia

E-mail: parya.fathi@monash.edu

RECEIVED
1 March 2021

REVISED
27 April 2021

ACCEPTED FOR PUBLICATION
21 May 2021

PUBLISHED
17 June 2021

Keywords: chipless RFID tags, conductive inks, industry laminates, screen printing, sintering temperature

Abstract

A chipless radio frequency identification (RFID) tag is a suitable low-cost alternative to any chip-based RFID one. The flexibility to use low-cost printing techniques makes chipless RFID a competitive technology. In this paper, we report an evaluation of the microwave performance of two different screen-printed chipless tags in the 3–6 GHz range. The tags were designed and screen printed on industry packaging laminates using nanoparticle conductive ink-paste supplied by ANP and InkTec companies. The measured microwave performance of tags was compared with simulated performance and printing parameters that influence the print quality, and eventually, the microwave response of the tags are discussed.

1. Introduction

Printed electronics (PE) have revolutionized the field of flexible electronics and gained popularity in the manufacturing of electronic devices such as large-area sensors [1], antennas [2], light-emitting diodes, transistors [3], radio frequency identification (RFID) tags [4]. Unlike the conventional fabrication method, where the solid copper sheets bonded to the substrates are etched to form the electrical tracks on the board, printing requires the metal particles to be in the form of inks. One of the benefits of printing is additivity, as it enables conductive structures to be manufactured simply by adding material layers. Furthermore, printing has been proven as a faster method than traditional manufacturing methods due to the reduction of the number of steps needed on a production line.

Printed tags in different applications such as wearable electronics for healthcare [5–7] and the packaging industry [8] require simplified fabrication method with reduced wastes. At the same time, low-cost and fast fabrication processes have attracted the researchers to investigate different printing technologies in the fabrication of RFID tags. A reader and a tag constitute the two main components of RFID technology. The tag is completely a passive device for the chipless RFID technologies without any integrated circuit (IC) on it [9]. The absence of IC in chipless RFID tags eliminates the IC fabrication and assembling costs. Consequently, tag costs are limited to the cost of the substrate and printing of the tag patterns, with different shapes and structures depending on the chosen tag configurations and encoding techniques that include time, frequency, hybrid, and image-based encoding. Substrate material cost can be considered negligible by using low-cost substrates such as paper and polymer films. Silver-based inks are generally expensive and therefore impose a severe constraint on the amount of ink that is used to print a unit area of a particular tag pattern. For this reason, small-sized tag patterns are preferred. This is a viable method to keep the overall printing cost low and printed tag bit density high.

The common printing technologies proposed for RFID tags printing can be categorized into general groups of contact and non-contact printing processes. Gravure and flexography [10] are introduced as contact printing, where the pattern wetted with the ink is brought in physical contact with the substrate. In contrast, inkjet and screen printing are introduced as non-contact printing, where the ink spreads on the substrate through nozzles in the inkjet printer or open pores on the screen in the screen printing method. A more thorough review of each printing method can be found in [11].

Among all printing techniques, screen-printing and inkjet printing have received greater attraction in the fabrication of chipless RFID tags owing to the simplicity of the printing technique, reduced waste material, and adaptability with the fabrication process. Inkjet printers are found to print electrical tracks with a low thickness of about 2–3.5 μm

[12, 13], often not sufficient to meet the tag conductivity requirement, especially for tags operating at low-frequency bands. At reduced frequencies, the minimum required thickness for electrical tracks increases due to the increase of skin depth. Screen printing as an alternative printing technique suggests obtaining a high printing aspect ratio and the ability to print lines with thickness values of >5 μm [14]. Line thickness is closely related to the electrical conductivity of the printed conductors. Thicker lines enable higher electrical conductivity. However, the screen printing technique has few limitations. The width of the lines that can be printed is limited to ~50 μm, which is considered a constraint compared to other printing techniques [14].

Screen printing has been reported in the fabrication of chipless RFID tags, and it is introduced as a fast fabrication technique compared to inkjet printing [15–18]. In [17], a three-bit dipole-shaped tag is designed and fabricated on the polyethylene terephthalate (PET) substrate using a screen printing method, where a conductive track with a thickness of 10 μm is obtained. A QR-like, 8-bit tag is also fabricated on the Melinex 401 CW PET substrate from DuPont Teijin Films using the screen printing method in [16]. In [18], an octagonal-shaped five-bit tag is fabricated on the flexible PET and paper substrates, and the effects of bending and folding are analyzed.

Although various printed chipless RFID tags and sensors are reported in the literature, the issues with different printing techniques and the parameters affecting the microwave responses of the printed tags were not comprehensively discussed. The aim of this paper is to study these parameters by screen printing two different frequency-coded chipless RFID tags. The configurations of the tags include a 2-bit retransmission configuration (circuit-based) and a 1-bit backscattered resonator-based configuration. These tags were deposited over few varieties of packaging substrates. The rest of the paper is organized as follows: section 2 covers details of the screen printing. It also includes a discussion on the substrate and conductive ink effects on the printing quality, which affects the performance of the chipless RFID tags. In section 3, the selected tag designs and their printing on different substrates using two different nanoparticle silver inks were discussed. Simulations of the microwave performance and measured tag responses are presented and discussed in section 4, and finally, section 5 covers the conclusions of our studies.

2. Screen printing

The output of the screen printing process is dependent on several factors. Among them, material characteristics are recognized as the key factor due to interactions that arise during the printing process on various substrate materials using inks of different compositions and, as a result, have a significant effect on the performance of the finished structure. Other parameters related to the printing process are the selection of the screen with an appropriate mesh size to obtain good printing resolution and ink thickness and the curing of the printed ink at a suitable temperature that needs to be carried out to obtain the electrical functionality of the printed patterns.

2.1. Substrate

Substrate's thickness, relative permittivity, and loss tangent are important properties that affect the microwave performance of the tags. The increase of substrate permittivity decreases bandwidth, resonance frequency, and the attenuation of the signal at the resonance frequency. However increase of loss tangent does not affect resonant frequency, while it increases the bandwidth and decreases the attenuation of signal at the resonance frequency. The substrate thickness has the least impact on the microwave performance of the tags, and it has been observed that with the increase of substrate thickness, bandwidth and the attenuation of signal at resonance frequency reduces very slowly, while the resonant frequency changes are small [19].

The physical properties of the substrate that affect the printing quality are the surface energy, surface roughness, and substrate melting point. The surface energy determines the substrate wettability for a particular ink. A substrate with low surface energy may not be able to hold the ink drops properly. To have a better printing quality, the surface energy of the substrate is suggested to be higher than the surface tension of the ink. Surface roughness is yet another parameter related to the substrate that impacts the adhesion of the ink to the substrate. Therefore, it is often helpful to determine the surface roughness of the substrates selected before printing so that it can be related to the surface tension of the ink after printing is completed. Melting point is another important physical property that constraints the sintering temperature after printing and accordingly limits the electrical conductivity.

2.2. Ink

The conductive printing inks are usually manufactured by mixing various components to enable good printing over a selected substrate materials. Functional inks include conductive metal pigments, solvent (aqueous or organic) that controls the dispersion of pigments, a polymer-based binder for keeping the pigments together, and additives that enhance adhesion of the ink pigments on the substrate. In screen printing, it is the most common practice to stick to flake-sized particle inks made from a mixture of functional metal and solvent-related components [14].

Table 1. Typical ink viscosities for different printing techniques.

Printing technique	Ink viscosity (cP)
Inkjet	1–20
Gravure	100–1000
Screen	500–5000
Flexo	50–500
Offset	100–10 000

The amount and type of metal particles of inks determine their conductivity. The silver-based inks are proven to demonstrate high conductivity. Another critical parameter that affects the conductivity is the thickness of the deposited inks on the substrate, directly related to their viscosity. Ink viscosities for different printing techniques are listed in table 1. In screen printing, inks have to withstand the shearing force applied over the ink to spread it over the screen. The amount of shearing force applied is controlled to ensure uniform ink spreading, resulting in good print quality [20]. Low viscosity inks lead to ink flow directly through screen openings prior to printing.

Inks with solvents that evaporate fast can cause clogging of the screen due to drying of the ink over the screen before dragging it over the screen. In PE applications, it is necessary to carefully select the ink composition in terms of its viscosity and surface tension, which in turn impact the print quality through the substrate-ink interface behavior when wet ink hits the substrate. The type of solvents used in ink formulations with functional inks such as silver and copper-based inks might affect the print quality due to its poor adhesion to the substrate surface.

The substrates with printed ink need to undergo thermal or other types of sintering process at suitable temperatures, to let the binders evaporate and connect the metal pigments forming continuous connected printed lines. Hence, sintering enhances electrical connectivity between metal particles of inks and promotes high-conductivity printed tracks. As it is going to be shown in this paper, by increasing the conductivity of the printed resonators, their radar cross section (RCS) level and resonant quality factor increase, which consequently enhances detection. Polymer substrates such as Nylon and Polypropylene are sensitive to the application of heat and therefore should be sintered at reduced temperatures. Alternatively, it is safe to use photon sintering for inks deposited on these substrates.

3. Printing of tags

The product details of silver inks used in screen printing in this paper are shown in table 2. Two low-cost screen printers supplied by Upart Equipment Limited, China (Price—$1000) were used to print the tags using a polyester screen with 140T mesh count. SCG Packaging Public Company Ltd, Thailand, kindly supplied the plastic and paper substrates for printing. The sintering conditions of the printed tags are shown in tables 3 and 4. The 125 μm Mylar-PET film was purchased from a local supplier with the sintering conditions shown later in table 5.

Table 2. Typical ink viscosities for different printing techniques.

Supplier	ANP	InkTec
Ink Code	DGP80-TES	TEC-PA-010
Type	Nano	Nano
Viscosity, cP	100 000–150 000	7000–7500
Ag-content, weight %	70–80	∼55
Diluting solvent	Alpha Terpineol	TEC-DA-010
Particle size, nm	Sub-micron	80–100
Specific resistivity, Ω cm	$\leqslant 3 \times 10^{10-5}$	$<6 \times 10^{10-6}$
Line width and thickness, μm	60–0, 10–15	$\geqslant$50, 1–2
Curing, °C (min) supplier data present work	120–150 (30) 140 (30)	120–170 (2–5) 140 (5)
Surface Tension, mN m^{-1}	54	54

Table 3. Technical information of plastic substrates.

Material	PET (A)	PVC (B)	Nylon (C)	PET (D)
Safe heating temperature in deg. C	<200	<150	<70	<70
Sintering temperature in deg. C and time in min.	140 (5)	100 (5)	70 (5)	70 (5)
Substrate, thickness, μm	35	89	81	53
Surface energy Fowkes, mN m^{-1}	42	39	34	51
Dyne level, #No	44	40	67	44

Table 4. Technical information of paper substrates.

Material	Clay coated paper (E)	Clay coated board (F)	Uncoated paper (G)
Safe heating temperature in deg. C	<100	<100	<100
Sintering temperature in deg. C and time in min.	100 (5)	100 (5)	100 (5)
Substrate thickness, μm	152	485	88
Surface energy (top): Fowkes, mN m^{-1}	42	39	51

Table 5. Details of substrate material properties, printing quality and measured electrical conductivities.

Substrate material	Substrate sintering conditions	Substrate surface energy (mN m^{-1})	Substrate surface roughness (μm)	Line width/gap discrepancy (μm)		Measured electrical conductivity (S m^{-1}) of 2-bit tag		Measured electrical conductivity (S m^{-1}) of 1-bit tag	
			Rp (pk-to-pk)	ANP	InkTec	ANP	InkTec	ANP	InkTec
Mylar PET	140 °C, 20 min	42	0.2	30	174	6.7E+05	1.0E+07	2.1+E05	5.2E+06
PET (A)	140 °C, 5 min	42	0.4	126	126	4.3E+05	6.7E+06	6.4E+04	3.8E+06
PVC (B)	100 °C, 5 min	39	0.7	126	126	1.6E+04	4.5E+06	3.5E+04	2.2E+06
Nylon (C)	70 °C, 5 min	34	0.3	222	174	1.1E+04	2.2E+06	—	—
PET (D)	70 °C, 5 min	51	0.3	222	126	1.4 E+04	5.0E+06	—	—
Clay-coated paper (E)	100 °C, 5 min	42	0.9	126	126	3.3E+04	1.8E+06	2.6E+04	2.1E+06
Clay-coated cardboard (F)	100 °C, 5 min	39	1.8	174	174	3.0E+04	2.4E+06	—	—
Uncoated paper (G)	100 °C, 5 min	51	2.2	78	174	7.4E+03	2.5E+06	—	—

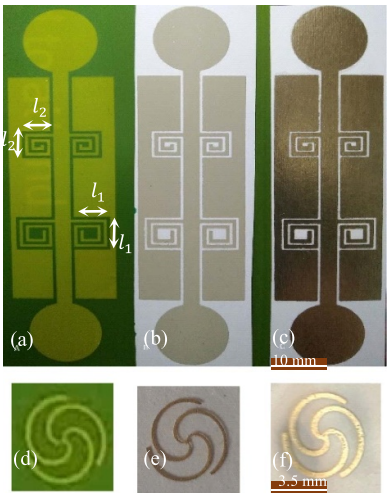

Figure 1. (a) 2-bit retransmission-based tag with receiving and transmitting disk-shaped antennas on stencil design with the printed tags shown in (b) ANP and (c) InkTec conductive ink on clay coated cardboard substrate. (d) 1-bit backscattered-based tag on stencil design with the printed tags in (e) ANP and (f) InkTec conductive ink on Mylar PET substrate.

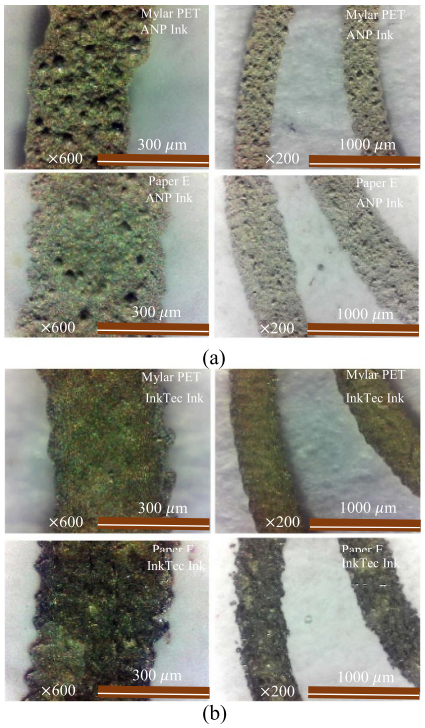

Figure 2. Microscopic image of printed tracks of (a) ANP ink and (b) Inktec ink on two different substrates of Mylar PET and Clay coated paper E.

In the current study, two different frequency coded tag designs were used. They are (1) a 2-bit retransmission configuration (circuit-based) and (2) a 1-bit backscattered resonator based configuration. Pictures of the tag designs are shown in figures 1(a) and (f). The pictures of the tags printed in ANP ink are shown in figures 1(b) and (e), and the pictures of the tags printed in InkTec are shown in figures 1(c) and (f).

In the 2-bit retransmission configuration, the spiral-shaped resonators were externally coupled to the ground plane of the coplanar waveguide and feed-line with a gap capacitance. Each resonator can only encode a single bit. The wireless communication takes place by means of two ultra-wideband (UWB) transmitting and receiving disk-shaped monopole antennas connected to the two ends of the waveguide [5]. The antennas exhibit Omni-directional radiation patterns with 0 dB gain.

In the 1-bit backscattered-based configuration, a three-armed spiral-shaped resonator handles the filtering, receiving, and transmission of the UWB signal using smaller size structures (7 mm × 7 mm) compared to a retransmission-based configuration with a relatively large design (20 mm × 80 mm).

Microscopic images in figure 2, taken with Maginon USB optical microscope with magnification of 200× and 600× from a three-armed spiral-shaped resonator printed on substrates of Mylar PET and Clay-coated paper E, show the quality of the prints and confirms the density of printed tracks. Only some parts of the edges of the lines are indented due to extra ink flow for the parts with thicker width or clogging of screen openings for the parts with thinner width.

4. Results and discussion

The surface tension of an ink dictates whether a coating will wet and spread over, or retract from, a solid surface. Surface tension is expressed as force per unit of width, as dynes cm^{-1} (or mN m^{-1}). Solvents, typically used in solvent-borne formulations, are in the 20–30 dynes cm^{-1} range.

Inks exhibit both an adhesive force that is a measurement of the degree of association of the coating for the substrate, and a cohesive force that is a measure of the degree of self-adhesion of the coating. The spreading coefficient is the difference between work of adhesion and work of cohesion. If work of adhesion is greater than work of cohesion, then spontaneous spreading occurs. If work of cohesion is greater than work of adhesion, then retraction occurs, forcing a surface defect, as the coating will preferentially associate with itself.

In addition to the surface tension of the ink, transfer and spreading of ink on a substrate depend on the squeeze force applied on the ink and the surface energy of the substrate receiving the ink. The substrate must have surface energy higher than the surface tension of the ink, with forces of attraction great enough to promote good transfer and spreading, and consequently, good adhesion. High ink viscosity is essential to enable controlled ink spreading on the screen and enables the best line resolution and good

print quality [20]. Additional factors affecting adhesion include release properties of the surface, substrate composition, and the substrate layer structure.

The line and gap width for the design shown in figure 1(a) was fixed at 600 μm, and the width for the design shown in figure 1(d) was fixed at 300 μm. Using ANP and InkTec conductive silver inks, the 2-bit retransmission-based tags were screen printed over Mylar-PET films (thickness = 125 μm), PET (A) PVC (B), Nylon (C), PET (D), clay coated paper (E), clay coated cardboard (F) and uncoated paper (G) packaging laminates. The printed tags on Mylar-PET were sintered at 140 °C for 20 min, and those printed on other laminates were sintered at suitable temperatures, as shown in tables 3 and 4. After ensuring reasonable microwave responses of the 2-bit tags from actual laboratory measurements, the substrates of Mylar-PET, PET (A), PVC (B), and clay coated paper (E) were considered as suitable substrates for the screen printing of the 1-bit backscattered-based tags.

4.1. Printing accuracy

The printing accuracy was established from the measured width of the printed lines, comparing it with the originally designed width of the lines, only in the direction parallel to the squeeze movement on the screen. The surface roughness, as well as the thickness of the printed lines, was measured by an Optical Surface Profiler. The sheet resistance was measured by a four-point probe resistivity meter (SRM10) supplied by Bridgetec. The electrical conductivity was calculated from the sheet resistance and measured thickness of the printed silver lines. The sintering conditions for the packaging laminates, their surface energy, roughness values, printed Line width/gap discrepancy, and calculated electrical conductivity for the two inks used are shown in table 5.

The results of table 5 show that the printing accuracy is high for samples printed on Mylar PET with ANP ink due to the high viscosity of the ink. However, no relation is observed between the surface energy or surface roughness and printing accuracy for plastic substrates. It is a standard practice in the printing industry to subject the plastic surface to a corona discharge treatment before printing wet inks over it. In this study, the surfaces of the plastic laminates were not corona discharge treated. For the case of the paper-based substrates, the highest printing accuracy is obtained for prints in ANP ink deposited on the uncoated paper with the highest surface energy.

4.2. Electrical conductivity

The magnitude of the electrical conductivity of printed tags was found to be higher for Mylar PET and PET (A) and is associated with the higher sintering temperature by which improvement in conductivity is expected. In general, the magnitude of the electrical conductivity of tags printed in InkTec ink is higher in comparison to tags printed in ANP ink. This is because InkTec ink is manufactured and sold as a 'binder-free' formulation, especially for PE applications. ANP ink is not a binder-free ink and contains organic resins acting as binders to keep the ink composition intact.

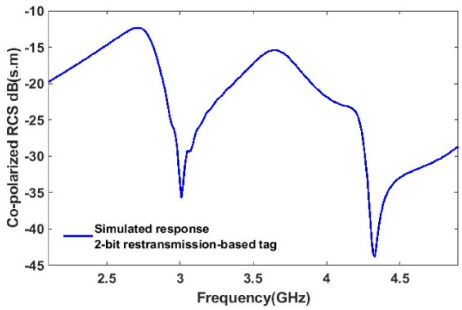

(a)

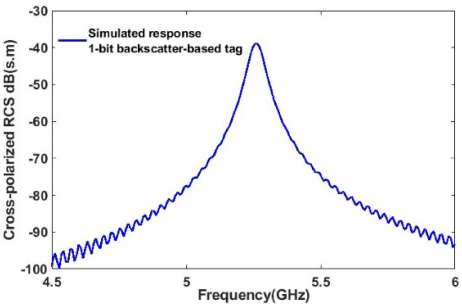

(b)

Figure 3. Simulated RCS response of (a) 2-bit retransmission-based tag and (b) 1-bit backscatter-based tag.

4.3. Simulations

Both proposed tags are simulated in CST Studio Suite, using its time-domain solver on the Taconic TLX-8 with 0.5 mm height and permittivity of 2.55. For a 2-bit retransmission-based tag (figures 1(a)–(c)), each spiral resonator will introduce a distinct stop-band resonance determined by the track width, width of the gap between the spiral arms, and the length of the spiral resonators [21]. The lengths l_1 and l_2 for the spirals shown in figure 1(a) were found to be 7.4 mm (large spiral) and 5.8 mm (small spiral), respectively. The width of the gaps between resonator arms is fixed at 0.6 mm. The co-polarized simulated RCS response of the 2-bit tag is shown in figure 3(a). In this figure, two distinct resonance frequency dips, one at 3.0 GHz and the other at 4.4 GHz, can be observed.

The resonance frequency of a 1-bit backscattered-based tag depends on the length of each spiraling arm. The equation for each arm is $r = a\sqrt{\varphi}$, $\varphi \geqslant 0$, where $'a'$ determines the degree of spiraling and $'\varphi'$ indicates the angle of spiraling in radians. For the resonator structure shown in figure 1(d), a and φ were found to be 1.6 and 4.9, respectively, and the width

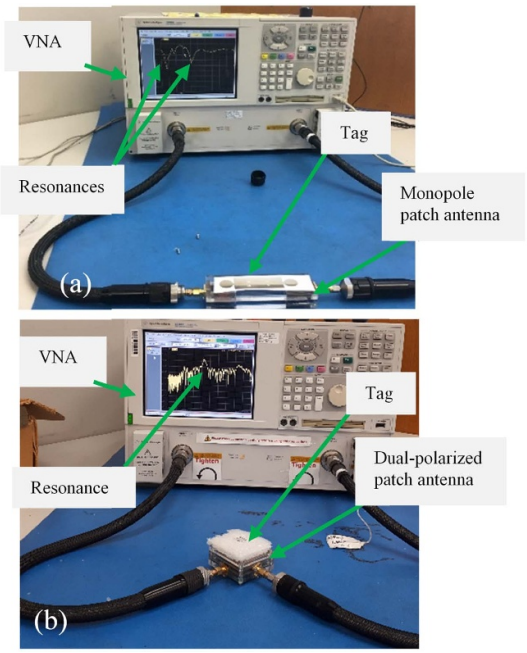

Figure 4. The measurement setup for (a) 2-bit retransmission-based tag and (b) 1-bit backscatter-based tag.

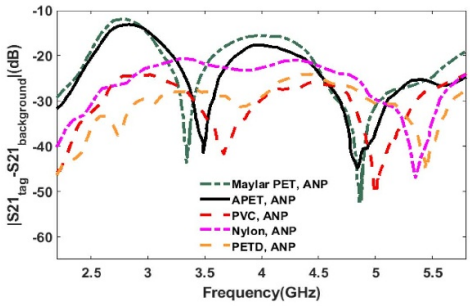

(a)

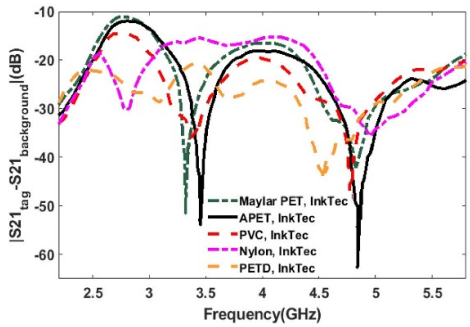

(b)

Figure 5. Measured microwave response of 2-bit retransmission-based tags printed on plastic films of Mylar-PET, PET-A, PVC, Nylon and PET-D using (a) ANP and (b) Ink Tec inks.

of each spiraling hand is fixed at 0.3 mm. The cross-polarized simulated RCS response of the tag is shown in figure 3(b), where a resonance peak at 5.26 GHz is observable.

4.4. Measurement setup

The microwave responses of the printed tags are measured by an Agilent Vector Network Analyser (VNA) using a setup shown in figure 4. Two monopole patch antennas with an operating frequency from 3.1 to 7 GHz [21] are used, as shown in figure 4(a), for the measurement of RCS response from the 2-bit retransmission-based tag. The disc-shaped monopole antennas of the tag are placed in the line of sight of the antennas. The return loss of these antennas was ∼10 dB in the operating bandwidth, and their gain varied between 1 and 2 dBi. In figure 4(b), a dual polarized patch antenna was used to transmit and receive the signals in the two polarizations, perpendicular to each other. The return loss and the isolation between the two ports of the antenna were found to be 10 dB and 28 dB, respectively, and the operating bandwidth of the antenna was found to be between 4.4 and 7 GHz with 8 dBi mid-band gain. Before measuring the microwave performance of the tags, with the setups shown in the figure, the background was measured to be subtracted from the tag responses using the VNA built-in function. The amplitude of the S_{21} was captured, indicating the co- and cross-polarized responses [22] of the 2-bit and 1-bit tags, respectively.

4.5. Microwave response of retransmission-based tag

The measured co-polarized response for the 2-bit retransmission-based tags printed on the plastic substrates using ANP and InkTec inks is shown in figures 5(a) and (b), respectively. The response of the tags printed on paper-based substrates is shown in figures 6(a) and (b).

The values of peak resonant frequencies collected from these plots is summarized in table 6 for ease of quick comparison of their performance vs substrate used. The substrate material dielectric constant shows influence on the microwave response and is also listed in the same table. A direct comparison of the measured RCS responses from figures 5 and 6 with the simulated response (figure 3(a)) show an occurrence of a frequency shift for all of the measured tags. Frequency shifts are directly related to the substrates' permittivity [19]. The loss tangent ($tan\delta$) is the property of the substrate that indicates the signal loss. It is one of the most significant factors controlling the quality factor of resonances in the spiral shaped resonator structures.

An analysis of the 2-bit tag response shows that the resonant dips for the tags printed on Nylon and PET (D) are wider, which relates to low quality factors associated with them and are barely detectable in the case of the first resonance dip. According to [23] and

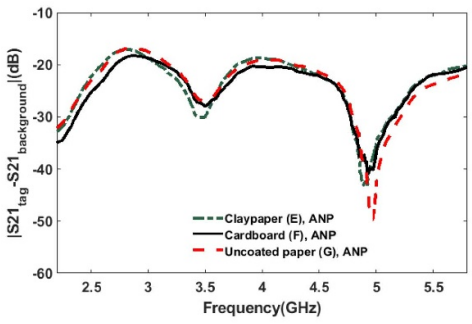

(a)

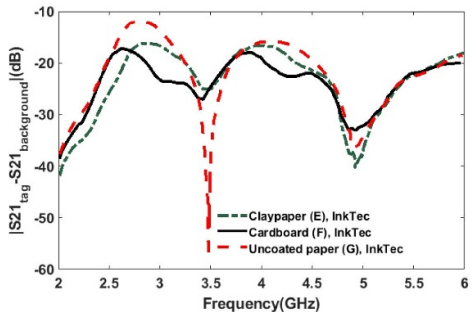

(b)

Figure 6. Measured microwave response of 2-bit retransmission-based tags printed on three varieties of paper laminates using (a) ANP and (b) Ink Tec inks.

Table 6. Frequency dips for the printed tags and dielectric constants of substrate materials.

Substrate material	Relative permittivity (ε_r) at frequency	Resonance dips, GHz (ANP)		Resonance dips, GHz (InkTec)	
Mylar PET	2.8 (1 GHz)	3.3	4.8	3.2	4.6
PET (A)	2.2	3.4	4.8	3.4	4.7
PVC (B)	3.2	3.6	4.8	3.3	4.6
Nylon (C)	2.8/3.1 (3.0/4.7 GHz)	3.9	5.3	3.2	4.8
PET (D)	2.2	3.8	5.4	3.6	4.4
Paper (E)	2–4	3.5	4.9	3.5	5.0
Card-board (F)	1.8 (2.5 GHz)	3.5	4.9	3.4	5.0
Paper (G)	2.2 (1 GHz)	3.5	5.0	3.5	5.0

[24], the total quality factor (Q_t) of a resonator structure can be obtained from following equation:

$$\frac{1}{Q_t} = \frac{1}{Q_{rad}} + \frac{1}{Q_c} + \frac{1}{Q_d} + \frac{1}{Q_{sw}}, \quad (1)$$

where Q_{rad} is the quality factor due to radiation loss and depends on the resonator structure, substrate height and permittivity ($Q_r \propto (\varepsilon_r/h)$); Q_c is the quality factor due to conductive losses ($Q_c = h\sqrt{\pi f \mu \sigma_c}$) and it is proportional to substrate height (h), operating frequency (f), and conductivity of the conductor (σ_c). Q_d is the quality factor due to the dielectric losses and it is inversely proportional to loss tangent ($Q_d = 1/\tan\delta$). Q_{sw} is the quality factor due to the surface wave losses and its value is negligible for all resonator structures deposited on a substrate with its height smaller than the resonator wavelength. Hence, it can be inferred that for the structures on substrates with smaller heights ($h \ll \lambda$), the quality factors associated with the dielectric and conductive losses and consequently, the loss tangent of substrates and the conductivity of the conductive tracks mainly limit the overall quality factor.

In the light of the above discussion and considering the data presented in tables 3–5, the low quality factor that is observable in the responses of tags printed on Nylon and PET (D) could be due to the higher loss tangent of these substrates compared to other substrates.

4.6. Microwave response of backscatter-based tag

1-bit backscatter-based tag is most desirable for real-world applications of chipless RFID due to its small size (7 mm × 7 mm). These tags were screen printed

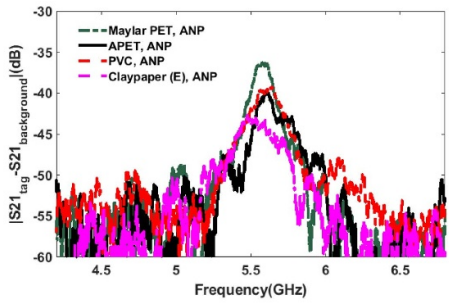

(a)

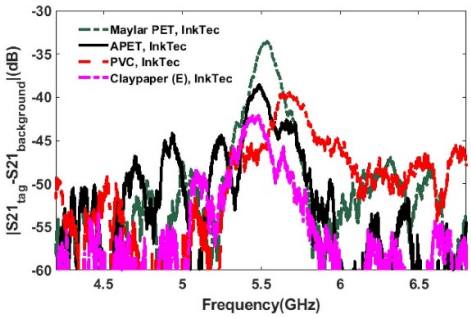

(b)

Figure 7. Measured microwave response of 1-bit backscatter-based tags printed on Mylar-PET, PET-A, PVC, and Clay paper (E) using (a) ANP and (b) Ink Tec inks.

Table 7. Frequency peaks for the printed tags and dielectric constants of substrate materials.

Substrate material	Relative permittivity (ε_r) at frequency	Resonance peaks, GHz	Resonance peaks, GHz
		ANP	InkTec
Mylar PET	2.8 (1 GHz)	5.6	5.5
PET (A)	2.2	5.6	5.5
PVC (B)	3.2	5.6	5.6
Paper (E)	2–4	5.6	5.5

on Mylar PET, APET, PVC, and Clay paper (E). The measured cross-polarized response for these tag printed on different substrates using ANP and InkTec inks is shown in figures 7(a) and (b), respectively. It is interesting to note that the line width of the printed tags in this configuration, is two times smaller than the minimum line width obtained in the 2-bit retransmission-based tag configuration and the overall size of the tag was found to be almost 16 times smaller than 2-bit retransmission-based structures.

The values of resonance frequency obtained from the measurements are listed in table 7 for comparison. The plots shown in figures 7(a) and (b) reveal that the amplitude of the signals are lower for tags printed in ANP ink compared to those printed in InkTec ink. The observed differences are associated with the conductivity of the printed tracks listed in table 5. It is also observed that the signal amplitude level is different for tags printed with the same ink on the different substrates. This is due to the sintering temperature limitations imposed by the substrate materials, most of which required lower temperature sintering to prevent damage to the substrate.

With a direct assessment of the quality factor of the resonant peaks in the 1-bit backscatter-based tag and resonant dips in the 2-bit retransmission-based tag, it could be inferred that the tags printed on Mylar-PET and A (PET) exhibited the best microwave performance because of sintering at 140 °C imparting maximum electrical conductivity to the printed tracks.

5. Conclusions

All the parameters affecting the printing quality and microwave responses of the tags has been highlighted by analyzing microwave performance of screen printed 2-bit retransmission based and 1-bit backscattered based tags. The tags were printed using two distinct nanoparticle silver based conductive inks on different substrates supplied by SCG. One of the inks is binder-free and the other was mixed with resin

based binder. The tags printed in binder free ink showed higher electrical conductivity over the tags printed in resin-based ink. Sintering temperature and time are set according to the information supplied by SCG for the different substrates as shown in table 5, and they posed a severe limitation on tag performance for all of the tags printed on substrates other than Mylar PET, where its sintering time is longer and sintering temperature is higher compared to other substrates.

Data availability statement

All data that support the findings of this study are included within the article (and any supplementary files).

This research is partly supported by the Australian Research Council's (ARC) Linkage Project grant LP1310144.

ORCID iDs

Parya Fathi https://orcid.org/0000-0002-9784-5610
Sika Shrestha https://orcid.org/0000-0002-6223-246X

References

[1] Chang W-Y, Fang T-H, Lin H-J, Shen Y-T and Lin Y-C 2009 A large area flexible array sensors using screen printing technology *J. Disp. Technol.* **5** 178–83
[2] Xiao G, Aflaki P, Lang S, Zhang Z, Tao Y, Py C, Lu P, Martin C and Change S 2018 Printed UHF RFID reader antennas for potential retail applications *IEEE J. Radio Freq. Identif.* **2** 31–7
[3] Khan S, Lorenzelli L and Dahiya R S 2014 Technologies for printing sensors and electronics over large flexible substrates: a review *IEEE Sens. J.* **15** 3164–85
[4] Jaakkola K, Ermolov V, Karagiannidis P G, Hodge S A, Lombardi L, Zhang X, Grenman R, Sandberg H, Lombardo A and Ferrari A C 2019 Screen-printed and spray coated graphene-based RFID transponders *2D Mater.* **7** 15019
[5] Preradovic S and Karmakar N C 2009 Design of fully printable planar chipless RFID transponder with 35-bit data capacity *2009 European Microwave Conf. (EuMC)* (IEEE) pp 13–6
[6] Healey A J, Fathi P and Karmakar N C 2020 RFID sensors in medical applications *IEEE J. Radio Freq. Identif.* **4** 212–21
[7] Vuorinen T, Vehkaoja A, Jeyhani V, Noponen K, Onubeze A, Kankkunen T and Mäntysalo M 2016 Printed, skin-mounted hybrid system for ECG measurements *2016 6th Electronic System-Integration Technology Conf. (ESTC)* (IEEE) pp 1–6
[8] Fathi P, Karmakar N C, Bhattacharya M and Bhattacharya S 2020 Potential chipless RFID sensors for food packaging applications: a review *IEEE Sens. J.* **20** 9618–36
[9] Aliasgari J, Forouzandeh M and Karmakar N 2020 Chipless RFID readers for frequency-coded tags: time-domain or frequency-domain? *IEEE J. Radio Freq. Identif.* **4** 146–58
[10] Shrestha S, Yerramilli R and Karmakar N C 2019 Microwave performance of flexo-printed chipless RFID tags *Flex. Print. Electron.* **4** 45003
[11] Shrestha S 2019 Practical implementation of chipless RFID system
[12] Khan M M, Tahir F A, Farooqui M F, Shamim A and Cheema H M 2015 3.56-bits/cm^2 compact inkjet printed and application specific chipless RFID tag *IEEE Antennas Wirel. Propag. Lett.* **15** 1109–12
[13] Herrojo C, Mata-Contreras J, Nunez A, Paredes F, Ramon E and Martin F 2017 Near-field chipless-RFID system with high data capacity for security and authentication applications *IEEE Trans. Microw. Theory Tech.* **65** 5298–308
[14] Suganuma K 2014 *Printing Technology Introduction to Printed Electronics* (Berlin: Springer) pp 23–48
[15] Betancourt D, Nair R, Haase K, Schmidt G, Bellmann M, Höft D, Hübler A and Ellinger F 2015 Square-shape fully printed chipless RFID tag and its applications in evacuation procedures *2015 9th European Conf. Antennas and Propagation (EuCaP)* (IEEE) pp 1–5
[16] Betancourt D, Barahona M, Haase K, Schmidt G, Hübler A and Ellinger F 2017 Design of printed chipless-RFID tags with QR-code appearance based on genetic algorithm *IEEE Trans. Antennas Propag.* **65** 2190–5
[17] Nair R, Barahona M, Betancourt D, Schmidt G, Bellmann M, Höft D, Plettemeier D, Hübler A and Ellinger F 2014 A fully printed passive chipless RFID tag for low-cost mass production *The 8th European Conf. Antennas and Propagation (EuCaP 2014)* (IEEE) pp 2950–4
[18] Betancourt D, Haase K, Hübler A and Ellinger F 2016 Bending and folding effect study of flexible fully printed and late-stage codified octagonal chipless RFID tags *IEEE Trans. Antennas Propag.* **64** 2815–23
[19] Islam M A and Karmakar N C 2015 Real-world implementation challenges of a novel dual-polarized compact printable chipless RFID tag *IEEE Trans. Microw. Theory Tech.* **63** 4581–91
[20] Pekarovicova A and Husovska V 2016 Printing ink formulations *Print. Polym. William Andrew Publ* pp 41–55
[21] Preradovic S 2010 Chipless RFID system for barcode replacement (Doctoral dissertation, Monash University)
[22] Fathi P, Aliasgari J, Babaeian F, Karmakar N C, Bhattacharya M and Bhattacharya S 2019 Chipless RFID tags: co-or cross-polar tag? *2019 IEEE Asia-Pacific Microwave Conf. (APMC)* (IEEE) pp 117–9
[23] Daliri A, Galehdar A, Rowe W S T, John S, Wang C H and Ghorbani K 2014 Quality factor effect on the wireless range of microstrip patch antenna strain sensors *Sensors* **14** 595–605
[24] Aliasgari J and Karmakar N C 2020 Mathematical model of chipless RFID tags for detection improvement *IEEE Trans. Microw. Theory Tech.* **68** 4103–15